Dalton Transactions

PAPER

View Article Online
View Journal

Cite this: DOI: 10.1039/c5dt01636c

Cyclometalation and coupling of a rigid 4,5-bis(imino)acridanide pincer ligand on yttrium†

Edwin W. Y. Wong and David J. H. Emslie*

An extremely rigid NNN-donor proligand, 4,5-bis{(diphenylmethylene)amino}-2,7,9,9-tetramethylacridan, H[AlMe$_2$] was prepared in five steps starting from 5-methyl-2-aminobenzoic acid and 4-bromotoluene. Reaction of intensely orange H[AlMe$_2$] with LiCH$_2$SiMe$_3$ formed deep blue Li$_x$[AlMe$_2$]$_x$ (x = 2 in the solid state), while reaction with [Y(CH$_2$SiMe$_3$)$_3$(THF)$_2$] (0.5 equiv.) afforded deep blue [Y(AlMe$_2$)(Alm′$_2$)] (**1**; Alm′$_2$ = an Alm$_2$ ligand cyclometalated at the *ortho*-position of one of the phenyl rings). Compound **1** slowly isomerizes to form green-brown **2**, which contains a single trianionic, hexadentate ligand that features one amine, two imine, and three amido donors. The acridanide backbone and one imine group in each of the original Alm$_2$ ligands is intact, but the two acridanide backbones are now linked by an isoindoline heterocycle. Yttrium in **2** is coordinated to six nitrogen donors and the *ortho* carbon of an isoindoline phenyl substituent. The intense colours of H[AlMe$_2$], Li$_x$[AlMe$_2$]$_x$ and **1** were shown by TD-DFT calculations to arise from charge transfer transitions from the HOMO, which is localized on the acridanide ligand backbone, to the LUMO and LUMO+1, which are localized on the imine substituents. The conversion of **1** to **2** was studied by UV-Visible absorption spectroscopy and is first-order with a half-life of 7.8 hours at room temperature.

Received 30th April 2015,
Accepted 26th May 2015

DOI: 10.1039/c5dt01636c

www.rsc.org/dalton

Introduction

Extremely rigid ligands offer the ability to precisely tailor the coordination environment around a metal center, providing potential advantages over more flexible ligands. Additionally, ligand donor atoms can be arranged so that they are biased to coordinate to a metal in a predetermined geometry, and the positions of bulky substituents can be fixed in place in order to stabilize reactive metal centers, prevent dimerization, and inhibit ligand decomposition pathways. The fixing of the coordination environment and steric bulk around a metal center may also allow for control of substrate orientation and recognition that is useful for designing new catalyst systems. However, in the organometallic chemistry of electropositive elements, these advantages can only be realized if both the ligand framework and its substituents are resistant to cyclometalation[1] and nucleophilic attack.[2]

The Emslie group has previously employed an extremely rigid dianionic pincer ligand, 4,5-bis(2,6-diisopropylanilido)-2,7-di-*tert*-butyl-9,9-dimethylxanthene (XA$_2$; Fig. 1), to isolate rare examples of neutral and cationic organothorium complexes supported by non-carbocyclic pincer ligands, including neutral [(XA$_2$)AnR$_2$] (An = Th or U; R = CH$_2$SiMe$_3$, CH$_2$CMe$_3$, CH$_2$Ph or ^{n}Bu)[3] and cationic [(XA$_2$)ThR(η^6-toluene)][B(C$_6$F$_5$)$_4$] (R = CH$_2$SiMe$_3$ or CH$_2$Ph).[4] These promising results in actinide chemistry motivated us to pursue analogous organo-rare earth complexes supported by extremely rigid pincer ligands. The primary targets of this research are cationic rare earth alkyl complexes due to their potential to catalyze a range of transformations such as ethylene and α-olefin polymerization,[5] hydroamination,[6] and alkyne dimerization.[7] However, compared to tetravalent thorium, trivalent rare earth metals necessitate the use of a monoanionic rather than a dianionic ancillary ligand in order to access cationic alkyl complexes.

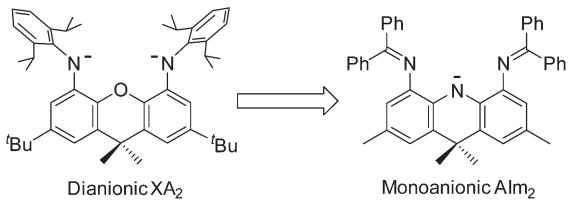

Fig. 1 Relationship between the XA$_2$ and Alm$_2$ ligands.

In an effort to develop a highly rigid, monoanionic pincer ligand that maintains the beneficial features of the dianionic

Department of Chemistry & Chemical Biology, McMaster University, 1280 Main Street West, Hamilton, Ontario L8S 4M1, Canada. E-mail: emslied@mcmaster.ca

†Electronic supplementary information (ESI) available: UV-Visible spectroscopy and DFT calculation data, and multinuclear and variable temperature NMR spectra. CCDC 1062734–1062737. For ESI and crystallographic data in CIF or other electronic format see DOI: 10.1039/c5dt01636c

XA_2 ligand, 4,5-bis{(diphenylmethylene)amino}-2,7,9,9-tetramethylacridanide (AIm_2), was developed, featuring a rigid tricyclic acridanide anion bearing pendant neutral imine donors (Fig. 1). The high rigidity of xanthene- and acridanide-backbone ligands stems from (a) the approximate planarity of the ligand backbone when coordinated to large, electropositive actinide[3,4] or rare earth (*vide infra*) elements, and (b) the absence of bonds which can rotate to move the ligand donor atoms closer or further away from one another. However, it should be noted that in combination with metals which are too small to fit well within the ligand binding pocket (*e.g.* Mg[8] or Li; *vide infra*), significant flexing of the ligand backbone may be observed.

Multidentate ligands incorporating both anionic amido and neutral imine donors have previously been shown to be able to stabilize both neutral and cationic organo-rare earth complexes without inhibiting productive reactivity. For example, the ligands in Fig. 2[9–15] have been used to develop neutral and cationic hydroamination catalysts (A, D, G and K),[10] cylic ester polymerization catalysts (B–D, G, J and I),[11] methyl methacrylate polymerization catalysts (G),[12] cationic isoprene polymerization catalysts (D, G, H, K and L),[13] cationic ethylene polymerization catalysts (D, F),[14] and isolable rare earth alkyl cations (A, D).[14,15]

The new AIm_2 ligand shares common functional elements with the amido/imine ligands in Fig. 2 but differs in that the substituent on the nitrogen atom of each imine group is part of the ligand backbone, as opposed to the ligands in Fig. 2 where the carbon atom of the imine functional group is attached to, or incorporated into, the ligand backbone. Herein, we report the synthesis of $H[AIm_2]$, reactions of $H[AIm_2]$ with $[Y(CH_2SiMe_3)_3(THF)_2]$ to form a cyclometalated and a ligand-coupled product, deprotonation of $H[AIm_2]$ to form $Li_x[AIm_2]_x$ (x = 2 in the solid state), and TD-DFT investigations into the origin of the unusual UV-Visible spectroscopic properties of these compounds.

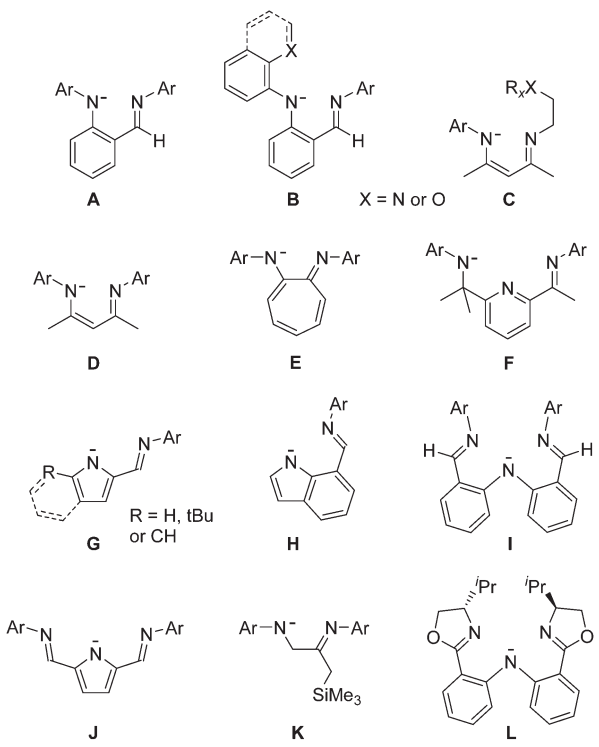

Fig. 2 Selected amido/imine ligands used to stabilize neutral and cationic organo-rare earth complexes. Only one resonance structure is shown for C–E.

Results and discussion

Ligand synthesis and structure

A six-step synthesis of the 4,5-dibromo-2,7,9,9-tetramethylacridan ligand precursor, $H[ABr_2]$, was previously reported by Du and co-workers.[16] However, a more efficient four-step route to $H[ABr_2]$ (Scheme 1) which avoids the use of diazomethane was pursued beginning from commercially available 5-methyl-2-aminobenzoic acid. This compound was esterified to form methyl 2-amino-5-methylbenzoate,[17] followed by Buchwald–Hartwig coupling with 4-bromotoluene to afford the previously reported ligand backbone intermediate, methyl 2-(*N*-(4-methylphenyl)amino)-5-methylbenzoate.[16] Following the published procedure with minor modifications, this intermediate was cyclized *via* tertiary alcohol formation and an intramolecular Friedel–Crafts alkylation to give 2,7,9,9-tetramethylacridan, $H[AH_2]$. Finally, $H[AH_2]$ was brominated to provide $H[ABr_2]$ according to the literature method.[16]

Synthesis of $H[AIm_2]$ was accomplished in 75% isolated yield *via* a Pd-catalyzed imination of $H[ABr_2]$ with benzophenone imine (Scheme 1).[18] The ^1H and ^{13}C NMR spectra of $H[AIm_2]$ in CD_2Cl_2 are consistent with the expected structure, and the empirical formula and bulk purity of $H[AIm_2]$ were

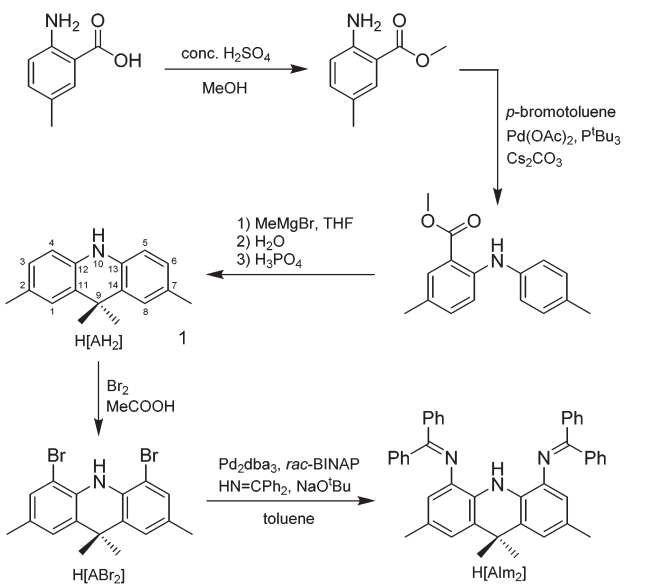

Scheme 1 Synthetic route to the $H[AIm_2]$ proligand.

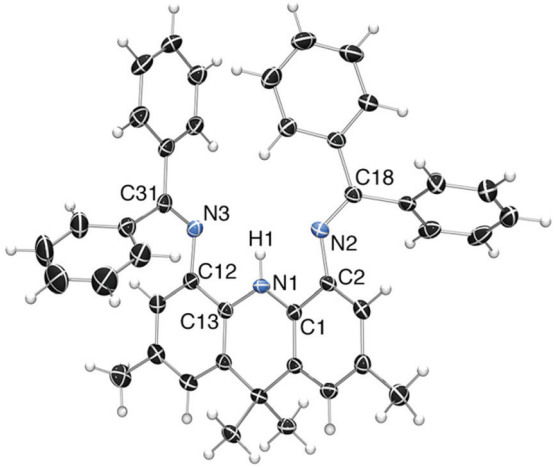

Fig. 3 Single crystal X-ray structure of H[AIm$_2$]. Thermal ellipsoids are set at 50% probability. Selected bond lengths [Å]: N1–C1 1.3782(17), N1–C13 1.3828(17), N2–C2 1.4155(16), N2–C18 1.2833(16), N3–C12 1.4250(16), N3–C31 1.2839(17).

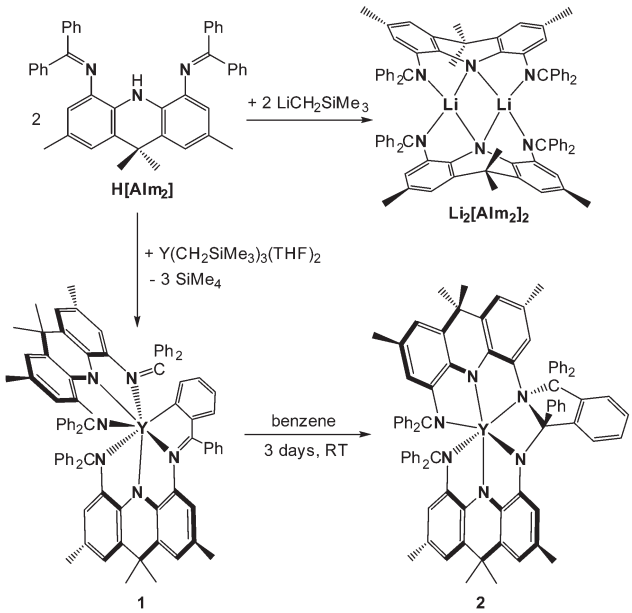

Scheme 2 Synthesis of **1**, **2** and Li$_2$[AIm$_2$]$_2$. In the structure of **2**, an interaction between yttrium and an *ortho* carbon atom of one of the isoindoline phenyl rings is not shown.

confirmed by elemental analysis. The identity of H[AIm$_2$] was further established by single crystal X-ray diffraction (Fig. 3), highlighting a planar acridan backbone with the N–H bond and the imine nitrogen atoms located in the plane, and bond distances within expected ranges.[19]

Synthesis and structure of yttrium complexes

Alkane elimination reactions between [Y(CH$_2$SiMe$_3$)$_3$(THF)$_2$][20] and H[AIm$_2$] were found to provide an effective ligand attachment method, with full consumption of the yttrium starting material requiring two equivalents of H[AIm$_2$]. In benzene-d_6, this reaction cleanly produced an intermediate dark blue product (**1**) which converted to a dark green-brown compound (**2**) at room temperature over the course of three days (Scheme 2).

The ^{1}H NMR spectrum of **1** does not contain signals attributable to a CH$_2$SiMe$_3$ group, indicating that ligand cyclometalation occurs rapidly with concomitant elimination of SiMe$_4$, either (a) directly from undetected [(AIm$_2$)$_2$Y(CH$_2$SiMe$_3$)], or (b) from undetected [(AIm$_2$)Y(CH$_2$SiMe$_3$)$_2$] prior to reaction with a second equivalent of H[AIm$_2$]; no intermediates were observed when the reaction was performed at −78 °C in d_8-toluene and warmed slowly to room temperature in the NMR spectrometer. Additionally, three Ar–CH_3 signals are observed for **1** in the ^{1}H and ^{13}C NMR spectra, indicating that one AIm$_2$ ligand has retained side-to-side symmetry while the second AIm$_2$ ligand has not, consistent with cyclometalation.

Small single crystals of [(AIm$_2$)(AIm′$_2$)Y]·(pentane)$_{0.5}$(toluene)$_2$ [**1**·(pentane)$_{0.5}$(toluene)$_2$; AIm′$_2$ = an AIm$_2$ ligand cyclometalated at the *ortho*-position of one of the phenyl rings] were obtained by layering a concentrated toluene solution of **1** with *n*-pentane and cooling to −25 °C. The crystal structure of **1** (Fig. 4) revealed a seven-coordinate yttrium complex with a highly distorted pentagonal bipyramidal geometry. In keeping with the ^{1}H and ^{13}C NMR spectra of **1**, one AIm$_2$ ligand is bound to the metal center in the expected tridentate fashion, while the second AIm$_2$ ligand has been cyclometalated at the

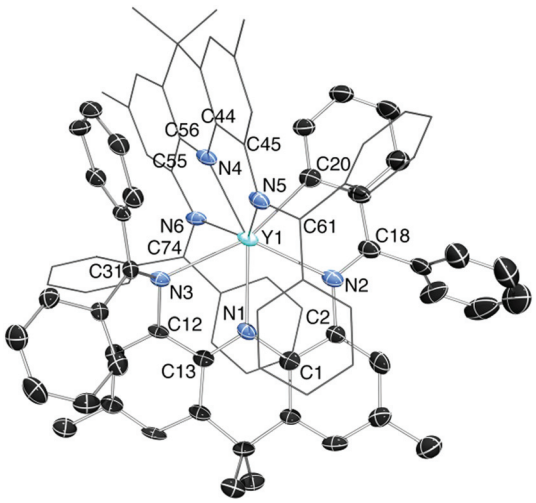

Fig. 4 Single crystal X-ray structure of **1**·(pentane)$_{0.5}$(toluene)$_2$. Hydrogen atoms and lattice solvent have been removed. Except for nitrogen atoms, the unactivated AIm$_2$ ligand is depicted in wireframe for clarity. Thermal ellipsoids are set at 50% probability. Selected bond lengths [Å]: Y1–N1 2.367(4), Y1–N2 2.529(4), Y1–N3 2.662(4), Y1–N4 2.358(4), Y1–N5 2.494(4), Y1–N6 2.475(5), Y1–C20 2.466(5), N1–C1 1.391(7), N1–C13 1.374(6), N2–C2 1.438(6), N2–C18 1.303(7), N3–C12 1.445(6), N3–C31 1.303(6), N4–C44 1.374(7), N4–C56 1.385(7), N5–C45 1.423(7), N5–C61 1.305(7), N6–C55 1.417(6), N6–C74 1.317(6).

ortho position of an imine phenyl ring, generating a dianionic, tetradentate ligand, AIm'_2, that lacks a C_2 axis.

The intact AIm_2 ligand backbone is essentially planar, with yttrium and the two imine nitrogen atoms located in the plane of the acridanide backbone. By contrast, the AIm'_2 dianion deviates slightly from planarity with an N(3)–N(1)–N(2)–C(20) torsion angle of 27.0°. The Y–C(20) distance of 2.466(5) Å is typical for an Y–C linkage to an *ortho*-cyclometalated phenyl ring; for example, the $Y–C_{aryl}$ distances in $[Cp_2Y\{o\text{-}C_6H_4\text{-}(CH_2CH_2NMe_2)\}]$,[21] $[\{o\text{-}NC_5H_3(C_6H_4)(CH{=}CMe\text{–}NAr)\}Y(NHAr)\text{-}(THF)]$,[22] $[\{o\text{-}C_6H_4(NAr)(Ph(C_6H_4)P{=}NMes)\}Y(\eta^3\text{-}CH_2CMeCHMe)\text{-}(THF)]$,[23] $[\{(o\text{-}NC_5H_3(C_6H_4)(CMe_2NAr))Y(\mu\text{-}H)(THF)\}_2]$,[24] and $[Y\{o\text{-}C_6H_4(CH_2CH_2NMe_2)\}_3]$[25] (Ar = 2,6-diisopropylphenyl; cyclometalated phenyl rings are shown in italics) range from 2.41 to 2.50 Å. The $Y–N_{diarylamido}$ bonds in **1** are 2.358(4) and 2.367(4) Å, lying towards the upper end of the typical range. However, a comparable $Y–N_{diarylamido}$ bond distance of 2.340(3) Å was reported for $[\{\kappa^3\text{-}N(o\text{-}C_6R_4(NHC))_2\}Y\{N(SiMe_3)_2\}_2]$ {NHC = $CN(NCH_2Ph)(CH)_2$}.[26]

The $Y–N_{imine}$ bonds in the AIm_2 monoanion in **1** are 2.475(5) and 2.494(4) Å. Crystallographically characterized rare earth imine complexes in which the nitrogen atom of the imine serves as the attachment point to the remainder of a multidentate ligand framework are $[Cp''(PhCN)Y(\mu\text{–}\kappa^2\text{:}\kappa^1\text{-}PhCH_2N\text{–}CPh{=}N)(\mu\text{–}\kappa^1\text{:}\kappa^3\text{-}N{=}CPh\text{–}N{=}CPh\text{–}N\text{–}CHPh\text{–}N{=}CHPh)YCp'']$ {Cp'' = $C_5Me_4(SiMe_3)$},[27] $[Cp^*_2Sm\{\kappa^2\text{-}N(SiMe_3)\text{–}CHPh\text{–}N{=}CHPh\}]$,[28] and 9-coordinate $[Sm\{\kappa^5\text{-}NH(CH_2CH_2N{=}CH\text{-}(2\text{-}NC_4H_3))_2\}\{\kappa^4\text{-}NH(CH_2CH_2N{=}CH(2\text{-}NC_4H_3))(CH_2CH_2N{=}CH\text{-}(2\text{-}NHC_4H_3)\}]$,[29] with $Ln–N_{terminal\text{-}imine}$ bonds of 2.517(3), 2.548(7) and 2.83(1) Å, respectively. With the exception of the latter bond distance, which is long due to the high coordination number, these distances are very similar to those in compound **1**, taking into account the larger ionic radius of Sm^{3+} *versus* Y^{3+} (0.96 *vs.* 0.90 Å for C.N. = 6).[30] Compared with the $Y–N_{imine}$ distances in the AIm_2 monoanion in **1**, the corresponding distances in the AIm'_2 dianion are significantly elongated [Y–N(2) = 2.529(4) Å; Y–N(3) = 2.662(4) Å], apparently due to steric restrictions imposed by the anionic amido and aryl donors of the rigid AIm'_2 ligand framework; N(2) is located between the two anionic donors, while N(3) is on the periphery. Nevertheless, all of the $Y–N_{imine}$ bonds in **1** fall within the broad range of $Y–N_{imine}$ distances reported in the literature; for example 2.429(2) and 2.457(2) Å in $[\{N(o\text{-}C_6H_4(CH{=}NAr))_2\}\text{-}Y(CH_2SiMe_3)_2]$ {L = bis(imino)diphenylamido},[5c] 2.483(2) Å in $[\{XylN\text{–}CH_2\text{–}C(CH_2SiMe_3){=}NXyl\}Y\text{-}(CH_2SiMe_3)_2(THF)]$ (Xyl = 2,6-dimethylphenyl),[6a] and 2.665(4) Å in $[\{NC_9H_5(8\text{-}O)\text{-}(2\text{-}CMe{=}NMes)\}YCl_2(dmso)_2]$ (NC_9H_5 = disubstituted quinoline).[31]

Compound **2** was prepared *via* the reaction of $[Y(CH_2SiMe_3)_3(THF)_2]$ with two equivalents of $H[AIm_2]$ in benzene followed by stirring for three days at room temperature. A total of 8 methyl (Ar–*Me* and C*Me*$_2$) signals are observed in the ^1H and ^{13}C NMR spectra of **2**, indicating the formation of a highly asymmetric product. X-ray quality crystals of **2**·$(benzene)_{3.35}$ (Fig. 5) were grown by layering a saturated benzene solution with pentane. Compound **2** is an isomer of **1** containing a single trianionic, hexadentate ligand that features one amine, two imine, and three amido donors. The acridanide backbone and one imine group of each of the original AIm_2 ligands is intact, but the two acridanide backbones are now linked by an isoindoline ring (Scheme 2). The yttrium center is coordinated to six nitrogen donors in an arrangement which leaves one face of the metal center open, possibly leading to an interaction with the *ortho* carbon [C(86)] of an isoindoline phenyl substituent positioned 2.904(2) Å from yttrium.

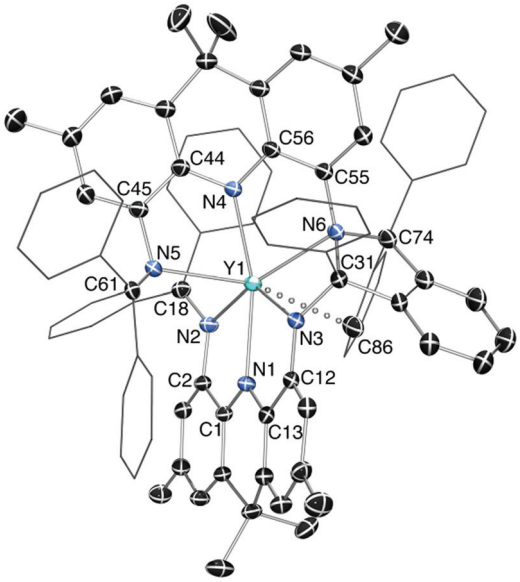

Fig. 5 Single crystal X-ray structure of **2**·$(benzene)_{3.35}$. Hydrogen atoms and lattice solvent have been removed, and phenyl substituents [except C(86)] are depicted in wireframe for clarity. Thermal ellipsoids are set at 50% probability. Selected bond lengths [Å]: Y1–N1 2.3281(16), Y1–N2 2.5236(18), Y1–N3 2.2020(18), Y1–N4 2.3258(17), Y1–N5 2.5388(17), Y1–N6 2.5858(18), Y1–C86 2.904(2), N1–C1 1.365(3), N1–C13 1.396(3), N2–C2 1.424(2), N2–C18 1.300(3), N3–C12 1.393(3), N3–C31 1.457(3), N4–C44 1.384(3), N4–C56 1.386(3), N5–C45 1.445(2), N5–C61 1.295(3), N6–C31 1.569(3), N6–C55 1.461(3), N6–C74 1.556(3).

The hexadentate, trianionic ligand contains two chiral centers in the isoindoline 5-membered ring, at N(6) and C(31), and crystals of **2**·$(benzene)_{3.35}$ contain a racemic mixture of SS and RR enantiomers. Diastereomers were not observed crystallographically or in the ^1H NMR spectrum, indicating that the constrained geometry of the yttrium-bound ligands during the rearrangement process (*vide infra*) only allows formation of the *rac* diastereomer. The C=N bonds of the unrearranged imines [1.295(3) and 1.300(3) Å] and the $C_{aryl}–N_{amido}$ distances [1.365(3) to 1.396(3) Å] in **2** are very similar to the corresponding bond distances in **1** (C=N = 1.30–1.32 Å; $C–N_{diarylamido}$ = 1.38–1.40 Å). The $C_{aryl}–N_{imine}$ distances in **2** [1.424(2) and 1.445(2) Å] are also comparable with those in **1** (1.41–1.45 Å), and are similar to the $C(31)_{sp3}–N(3)_{amido}$ and $C(55)_{aryl}–N(6)_{sp3}$ bonds to the isoindoline ring in **2** [1.457(3) and 1.461(3) Å, respectively]. By contrast, the C(31)–N(6) and C(74)–N(6) distances within the isoindoline ring in **2** are substantially elongated at 1.569(3) and 1.556(3) Å, respectively. Presumably

for steric reasons, these distances are longer than the corresponding C–N distances of 1.50–1.53 Å in [{O(*o*-C_6R_4)CH═N–CHPh–CHPh–N(CH_2)$_2$(*o*-C_6H_4)}MX_n] {MX_n = $TiCl_3$ and NiCl}, which contain an isoindoline heterocycle free from substituents on carbon.[32]

The Y–$N_{diarylamido}$ distances in **2** [Y(1)–N(1) = 2.3281(16) Å and Y(1)–N(4) = 2.3258(17) Å] are slightly shorter than the Y–$N_{diarylamido}$ distances in **1**, while the Y–N_{imine} bonds [Y(1)–N(2) = 2.5236(18) Å and Y(1)–N(5) = 2.5388(17) Å] are slightly longer than the Y–N_{imine} bonds to the unaltered AIm_2 ligand in **1**. These differences are ostensibly the result of geometric constraints imposed by the hexadentate ligand framework in **2**. The alkylarylamido donor, N3, resulting from the ligand coupling and rearrangement is trigonal planar [sum of bond angles around N3 = 358.88(25)°] with a Y(1)–N(3) distance of 2.2020(18) Å. This Y–$N_{alkylarylamido}$ distance is substantially shorter than the Y–$N_{diarylamido}$ bonds in **1** or **2** [2.3258(17)–2.367(4) Å], consistent with the enhanced donor ability of an alkylarylamido *versus* a diarylamido group; for comparison the Y–$N_{alkylarylamido}$ distance in [{κ^3-ArNCMeCHCMeN(CH_2)$_2$$NMe_2$}-Y(NHAr){N(Xyl)$CH_2$Ph}] {Xyl = 2,6-dimethylphenyl; Ar = 2,6-diisopropylphenyl} is 2.213(2) Å.[33]

The amine donor, N6, is pyramidalized with the sum of the C–N–C bond angles around N6 equal to 338.38(27)°. There are no crystallographic reports of an isoindoline donor bound to a rare earth element. However, the Y–N distances to the trialkylamine donors in [{κ^3-ArNCMeCHCMeN(CH_2)$_2$$NMe_2$}Y(NHAr)(κ^2-am^{iPr})] {Ar = 2,6-diisopropylphenyl; am^{iPr} = CH(N^{i}Pr)$_2$}[33] and [{κ^4-N(CH_2(*o*-C_5H_4N))-($CH_2CH_2NSiMe_3$)$_2$}Y(κ^2-am^{TMS,Ph})] {am^{TMS,Ph} = CPh($NSiMe_3$)$_2$}[34] are 2.511(3) and 2.557(3) Å, respectively, approaching the Y(1)–N(6) distance of 2.5858(18) Å in **2**. The metrical parameters of **2** are therefore in agreement with the identification of the hexadentate ligand as a tris(amido)-mono(amino)-bis(imino) donor.

In an attempt to disfavor ligand cyclometalation and rearrangement, a bulkier variant of AIm_2 with the phenyl substituents replaced with mesityl substituents was pursued. However, a suitable catalyst system[18b,35] for the Pd-catalyzed imination of H[ABr_2] with 2,2′,4,4′,6,6′-hexamethylbenzophenoneimine[36] could not be found. The reaction of [Y(CH_2SiMe_2Ph)$_3$(THF)$_2$][37] with one equivalent of H[AIm_2] in benzene-d_6 was also performed. However, **1** formed rapidly as the major product, indicating that the bulkier CH_2SiMe_2Ph ligand is not able to favor the formation of a mono-ligated bis-(alkyl) complex or to prevent AIm_2 ligand cyclometalation at room temperature.

UV-visible absorption spectroscopy and TD-DFT calculations

H[AIm_2], has an intense orange colour in solution and in the solid state, and the UV-vis absorption spectrum of H[AIm_2] in benzene exhibits a broad absorption band in the visible region with an absorption maximum at 438 nm (ε = 4640 L mol^{-1} cm^{-1}; Fig. 6). Time-dependent density functional theory calculations (TD-DFT, PCM benzene) were used to probe the origin of the intense orange colour of H[AIm_2]. The ground-state geometry of H[AIm_2] was optimized using a long range corrected

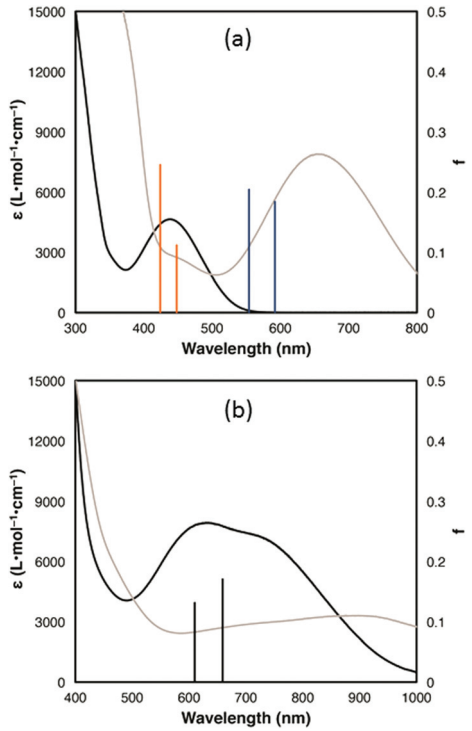

Fig. 6 (a) Absorption spectra of H[AIm_2] (black) and Li[AIm_2] (gray) in benzene; calculated high oscillator strength transitions for H[AIm_2] and Li[AIm_2] are shown as orange and blue lines, respectively. (b) Absorption spectra of **1** (black) and **2** (grey) in benzene; for **1**, calculated transitions with high oscillator strengths are shown as vertical black bars. In each plot, the *y*-axis on the left is the experimental extinction coefficient while the *y*-axis on the right is the calculated oscillator strength for each transition.

functional, CAM-B3LYP, with the default parameters (μ = 0.33, α = 0.19, β = 0.46) and the 6-31G* basis set, yielding a structure which closely mirrors the X-ray crystal structure. The μ, α, and β parameters of the CAM-B3LYP functional were then tuned according to the method reported by Nakano *et al.*[38] to more accurately reproduce the excited state energies of H[AIm_2]; values of μ = 0.15, α = 0.15, and β = 0.85 for CAM-B3LYP resulted in energies for the transitions that are in good agreement with the experimental spectrum (Fig. 6). The TD-DFT calculations predict two intense electronic transitions from the HOMO to the LUMO and the LUMO+1. The HOMO is primarily centered on the acridan ligand backbone, with the largest atomic contribution (25%) from the central nitrogen atom. By contrast, the LUMO and LUMO+1 are mostly centered on the N═CPh_2 substituents with the largest atomic contributions from the imine carbon atoms (10.5% and 11.5%), indicating that charge transfer transitions are responsible for the intense orange colour of H[AIm_2] (Fig. 7). This assignment is in keeping with the molecular structure of H[AIm_2], which bears resemblance to a donor–(π-bridge)–acceptor organic dye, such as those used in dye-sensitized solar cells.[39]

The intense blue and green-brown colours of **1** and **2** are highly unusual for d^0 yttrium(III) complexes; in benzene, **1**

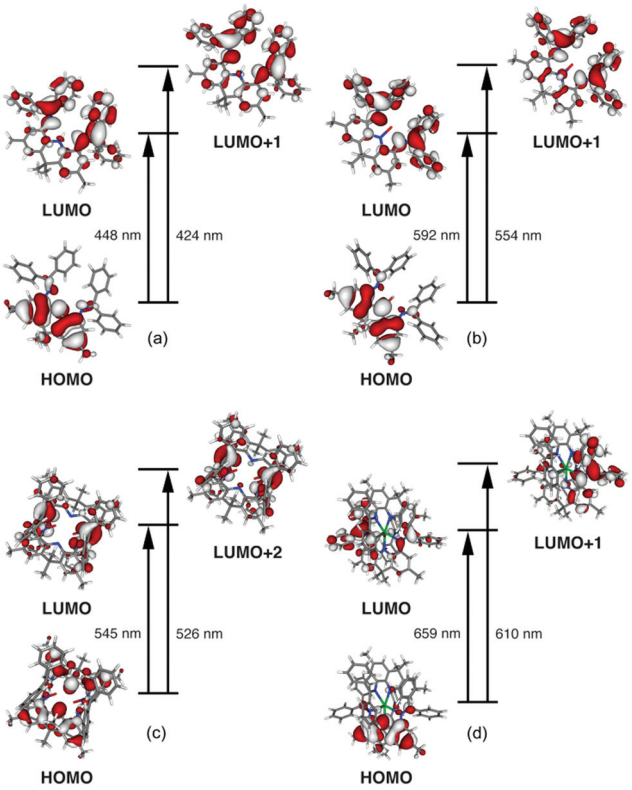

Fig. 7 Molecular orbital isosurfaces and TD-DFT transition energies for (a) H[AIm$_2$], (b) Li[AIm$_2$], (c) Li$_2$[AIm$_2$]$_2$, and (d) yttrium compound **1**.

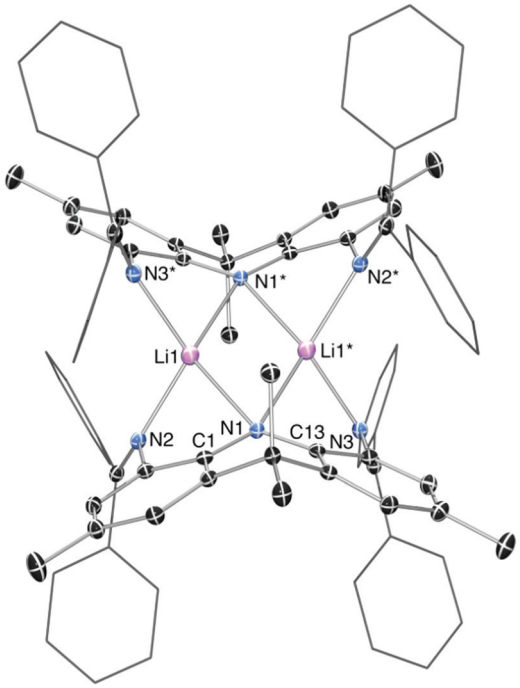

Fig. 8 Single crystal X-ray structure of Li$_2$[AIm$_2$]$_2$·toluene. Hydrogen atoms and lattice solvent have been removed, and phenyl substituents are depicted in wireframe for clarity. Thermal ellipsoids are set at 50% probability. Selected bond lengths [Å]: Li1–Li1* 2.474(6), Li1–N1 2.134(3), Li1*–N1 2.140(3), Li1–N2 2.095(3), Li1*–N3 2.089(3).

shows a broad absorption maximum at 637 nm (ε = 7911 L mol^{-1} cm^{-1}), while **2** shows a broad absorption that spans the visible range with a λ_{max} at 898 nm (ε = 3299 L mol^{-1} cm^{-1}) (Fig. 6b). Furthermore, it was found that deprotonation of H[AIm$_2$] with one equivalent of LiCH$_2$SiMe$_3$ in toluene gave dark blue Li$_2$[AIm$_2$]$_2$ (Scheme 2) with λ_{max} at 654 nm (ε = 7889 L mol^{-1} cm^{-1}) in benzene (Fig. 6a).

X-ray quality crystals of Li$_2$[AIm$_2$]$_2$·toluene were grown by layering pentane onto a toluene solution. The single crystal X-ray structure (Fig. 8) shows that Li[AIm$_2$] dimerizes in the solid state with a center of inversion midway between N(1)–N(1)*, rendering each monomeric unit crystallographically equivalent. Compared to the relatively flat ligand backbones of H[AIm$_2$], **1**, and **2**, the ligand backbone in Li$_2$[AIm$_2$]$_2$ has a 139° angle between the two aryl rings, and the central nitrogen-containing ring adopts a boat conformation. The Li(1)–Li(1)* distance of 2.474(6) Å is shorter than the reported distance of 2.79(1) Å[40] for [Li$_2${μ-1κ^2:2κ^2-N(PPh$_2$NSiMe$_3$)$_2$}$_2$], which exhibits similar connectivity to Li$_2$[AIm$_2$]$_2$, but is similar to the Li–Li distance of 2.494(6) Å in [Li$_2${μ-1κ^2:2κ^2-N(SiMe$_2$NEt$_2$)$_2$}$_2$] which features an acute Li–Si–Si–Li torsion angle of 38° around the central anionic nitrogen donors.[41]

The geometry at lithium is distorted tetrahedral with a 63.5° angle between the N(1)–Li(1)–N(2) and the N(1)*–Li(1)–N(3)* planes. The acridanide nitrogen donor, N(1), adopts an unusual distorted square planar geometry with Li(1)–N(1)–Li(1)*, Li(1)–N(1)–C(1), Li(1)*–N(1)–C(13) and C(1)–N(1)–C(13) angles of 70.74(14)°, 85.87(12)°, 86.56(12)° and 112.15(13)°, respectively. The angle between the Li(1)–N(1)–Li(1)* and C(1)–N(1)–C(13) planes is 24.5°, and the Li(1)–C(1)–C(13)–Li(1)* torsion angle between the four atoms bound to N(1) is just 2.0°. The unusual geometry at N(1) is suggestive of a 3c-2e Li(1)–N(1)–Li(1)* bonding interaction, and long Li–N$_{amido}$ distances support this conclusion; the Li(1)–N(1)$_{amido}$ and Li(1)*–N(1)$_{amido}$ distances are 2.140(3) and 2.134(3) Å, respectively, while the Li(1)–N(2)$_{imine}$ and Li(1)*–N(3)$_{imine}$ bonds are 2.095(3) and 2.089(3) Å. These bond distances follow the same trend as the average Li–N$_{bridging}$ [2.250(5) Å] and Li–N$_{non\text{-}bridging}$ [1.997(5) Å] distances reported for [Li$_2${μ-1κ^2:2κ^2-N(PPh$_2$NSiMe$_3$)$_2$}$_2$].[40]

TD-DFT calculations using the CAM-B3LYP functional (μ = 0.15, α = 0.15, and β = 0.85) and 6-31G* basis set for the Li[AIm$_2$] monomer and Li$_2$[AIm$_2$]$_2$ dimer predict a red-shift of λ_{max} relative to H[AIm$_2$]. However, only monomeric Li[AIm$_2$] afforded computed transition energies in reasonable agreement with experimental results (Fig. 6 and 7). In solution, it is likely that compound Li[AIm$_2$] exists as a monomer and/or a dimer, rather than a well-separated ion pair, and from these two possibilities, TD-DFT calculations suggest that a monomeric species is dominant. The experimental λ_{max} for solutions of Li[AIm$_2$] is also nearly identical in benzene and THF (654 *vs.* 652 nm), providing support for the predominance of a

monomeric species in both solvents. As with H[AIm$_2$], calculations on all three species predict intense charge transfer transitions from the HOMO to the LUMO and the LUMO+1/LUMO+2; the HOMO is centered primarily on the ligand backbone and the LUMO and LUMO+1/LUMO+2 are centered on the imine substituents (Fig. 6 and 7).

TD-DFT calculations were also carried out on **1** using the tuned CAM-B3LYP functional with LanL2DZ (Y) and 6–31G* (C, N, H) basis sets, yielding computed electronic transition energies close to experimental values (Fig. 6). The HOMO is mostly based on the ligand backbone of the unactivated AIm$_2$ ligand, whereas the LUMO and LUMO+1 are located primarily on the N=CPh$_2$ substituents of this ligand, each with a small contribution from an yttrium d orbital (Fig. 7). Therefore, the colour of **1** originates primarily from charge transfer within the intact AIm$_2$ ligand in **1**.

Kinetics and proposed mechanism for the formation of 2

In the conversion of **1** to **2**, it is likely that the imine carbon of the intact AIm$_2$ ligand in **1** inserts into the Y–C bond to form **1′**. Compound **2** can then be formed by a second 1,2-insertion involving the newly formed amido nitrogen and the imine carbon bound to the cyclometalated phenyl substituent, thereby generating the isoindoline ring that links the two acridanide moieties (Scheme 3).

Conversion of **1** to **2** was monitored by recording an absorption spectrum every 30 minutes from 0.5 hours to 60 hours after **1** was dissolved in benzene (Fig. 9). The absorption spectra were deconvoluted (see ESI†) to extract the absorbance of **1** at 630 nm since the absorbance of **2** at 630 nm is non-zero. Since, no intermediates are observed spectroscopically, $k_2 \gg k_1$ in Scheme 3, a first-order rate law can be applied as a close approximation for the rearrangement of **1** to **2**. The observed rate constant for the reaction is 0.089 h^{-1}, giving a half-life of 7.8 hours at room temperature (see Fig. S1 in ESI† for a plot of ln[A$_1$] *vs.* time (A_1 = absorbance of **1**); Eyring analysis was not attempted since the reaction is slow at room temperature and does not proceed cleanly above room temperature). A unimolecular process is consistent with the proposed intramolecular mechanism, ruling out intermolecular ligand transfer processes.

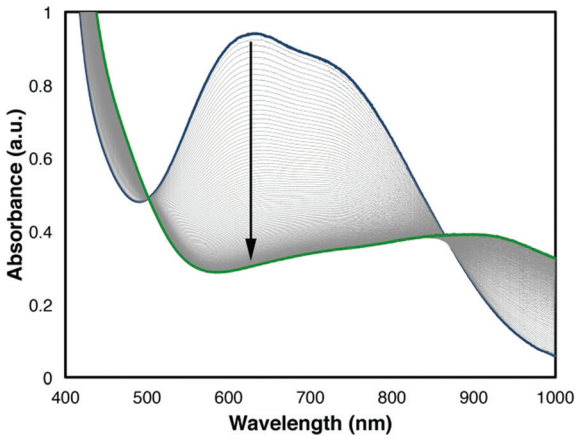

Fig. 9 Absorption spectra for the conversion of **1** to **2** recorded from 0.5 to 60 h in benzene.

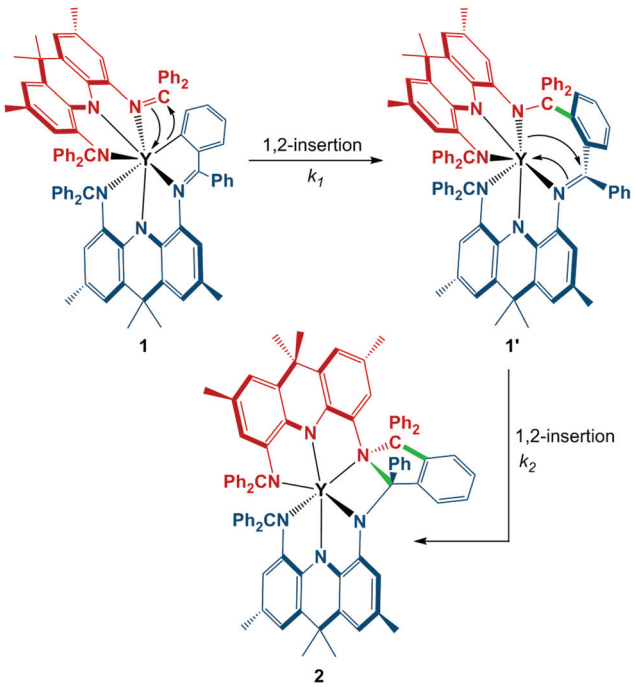

Scheme 3 Proposed reaction pathway for conversion of **1** to **2**.

Conclusions

An extremely rigid acridanide proligand, H[AIm$_2$], has been prepared and deprotonated to form Li[AIm$_2$]. The proligand is intensely orange coloured while the lithiated ligand is deep blue; these colours were found to originate from charge transfer transitions from the ligand backbone to the imine substituents, highlighting the structural relationship between H[AIm$_2$] and Li[AIm$_2$] and donor-pi-acceptor dyes. Addition of two equivalents of H[AIm$_2$] to [Y(CH$_2$SiMe$_3$)$_3$(THF)$_2$] rapidly generated cyclometalated bis(ligand) complex **1**. This deep blue compound undergoes a two-step intramolecular ligand coupling process to form green-brown **2** which contains a hexadentate tris(amido)-mono(amino)-bis(imino) trianion featuring an isoindoline moiety bridging between the two acridanide ligand backbones. As with H[AIm$_2$] and Li[AIm$_2$], the intense colour of **1** was calculated to originate from ligand-based charge transfer transitions. Attempts to synthesize stable dialkyl yttrium AIm$_2$ complexes using AIm$_2$ proved unsuccessful, even using bulkier CH$_2$SiMe$_2$Ph ligands. The 2,7,9,9-tetramethylacridanide ligand backbone is expected to provide a versatile platform for the development of new highly rigid pincer ligands. Future work will target acridanide pincer ligands incorporating neutral donor substituents that are less

prone to cyclometalation and nucleophilic attack, with a view towards the synthesis of robust neutral and cationic organo-rare earth complexes.

Experimental

General procedures

All manipulations of oxygen- or moisture-senstive materials were carried out under an atmosphere of argon in an Innovative Technology PureLab HE glovebox, MBraun UNIlab glovebox, or using standard Schlenk techniques. All glassware was rigorously dried overnight at 120 °C and cooled under vacuum before use.

Caesium carbonate was dried overnight at 70 °C under vacuum. Methyl-2-amino-5-methylbenzoate was prepared according to a published procedure.[17] 1,8-Dibromo-3,6,9,9-tetramethyl-9,10-dihydroacridine was synthesized from 3,6,9,9-tetramethyl-9,10-dihydroacridine using a reported procedure.[16] $Y(CH_2SiMe_3)_3(THF)_2$ [20] and $Y(CH_2SiMe_2Ph)_3(THF)_2$ [37] were synthesized according to published procedures. $LiCH_2SiMe_3$ was received as a 1.0 M solution in pentane, volatiles were removed *in vacuo*, and the remaining solid was collected and stored at −30 °C in a glovebox. All other reagents were purchased from commercial sources and used as received.

Pentane, benzene, and THF were dried and distilled at atmospheric pressure from sodium benzophenone ketyl; sodium was used to dry toluene. Unless otherwise noted, all anhydrous solvents were stored over an appropriate drying agent prior to use (THF, toluene, and C_6D_6 over Na/Ph_2CO; pentane over Na/Ph_2CO/tetraglyme).

All NMR spectra were collected on a Bruker DRX-500 or an AV-600 spectrometer. Chemical shifts for ^1H NMR spectra were referenced to residual ^1H NMR resonances of the deuterated solvent and ^{13}C NMR spectra were referenced to ^{13}C NMR resonances of the deuterated solvent.[42] All chemical shifts are reported relative to tetramethylsilane.

Peak assignments for all new compounds were made using ^1H, $^{13}C\{^1H\}$, DEPT-135, DEPT-q, COSY, HSQC and HMBC NMR experiments. TOCSY NMR was also used to aid in the assignment of the ^1H NMR spectra of **1** and **2**. In the ^{13}C NMR spectrum of compound **1**, 19 of the 25 expected Ar–CH peaks and 18 of the 19 expected quaternary Ar peaks were located. In the ^{13}C NMR spectrum of compound **2**, 30 of the 39 expected Ar–*C*H peaks, and 23 of the 25 expected quaternary Ar peaks were located. The remaining peaks were presumably obscured by coincidental overlap with other aryl peaks, given the large number of inequivalent aryl carbon environments (44 for **1** and 64 for **2**). These missing peaks could not be located in 2D HSQC or HMBC NMR experiments.

Assignments of the resonances in the NMR spectra were made according to the numbering scheme for acridines, as illustrated in Scheme 1.[43] For compound **2**, C_6H_5 ring A, and aryl rings B and C are rings in which all protons are inequivalent, and rings labeled α, β, γ and δ indicate the four aryl rings of the acridanide backbones. We were not able to identify which phenyl rings in the structure of **2** correspond to rings A–C, or which acridanide backbone aryl rings correspond to α, β, γ and δ.

UV-Vis absorption spectra were recorded at ambient temperature on a Varian Cary 50 Probe Spectrophotometer in a 1 cm quartz cell equipped with a Chemglass CHEM-VAC™ CHEM-CAP® valve. Elemental analyses were performed on a Thermo (Carlo Erba) Flash 2000 Elemental Analyzer at London Metropolitan University.

Computational methods

DFT and TD-DFT calculations were performed using Gaussian 09 (Revision D.01).[44] Geometry optimizations were performed using the CAM-B3LYP functional,[45] the 6-31G* basis set (C, H, N, Li),[46] and LanL2DZ basis set (Y).[47] Frequency calculations at the same level of theory confirmed that the optimized structures were located at a minimum on the potential energy surface. The same basis sets were used for single-point calculations, but the parameters of the CAM-B3LYP functional were modified to $\mu = 0.15$, $\alpha = 0.15$, and $\beta = 0.85$ from the default parameters of $\mu = 0.33$, $\alpha = 0.19$, $\beta = 0.46$. The energies and intensities of the 10 lowest energy electronic transitions were calculated by TD-DFT[48] using the same functional/basis set combinations employed for the single-point calculations and a polarized continuum model (PCM) for benzene.[49] AOMix[50] was used for determining atomic orbital compositions employing Mulliken Population Analysis.

X-ray crystallographic analyses were performed on a SMART APEX II diffractometer with a 3 kW Sealed tube Mo generator in the McMaster Analytical X-Ray (MAX) Diffraction Facility. Temperature was regulated using an Oxford Cryosystems Cryostream. Suitable crystals were coated in Paratone oil inside a glovebox ($Li_2[AIm_2]_2$, **1**, and **2**) or in air ($H[AIm_2]$), mounted on a MiTeGen head, and then placed in the cold stream of the diffractometer. Details of the data reduction and absorption correction can be found in the CIF. Structures were solved using SIR92[51] and refined by least-squares procedures in CRYSTALS.[52] The hydrogen bound to the nitrogen in $H[AIm_2]$ was located in the difference map and refined isotropically without other restraints. All other hydrogen atoms were placed in idealized geometric positions and linked to their respective atoms using a riding model during refinement. The isotropic temperature factor of each hydrogen atom was initially set to 1.2 times that of the atom it is bonded to and then the temperature factors of the hydrogen atoms were linked during refinement. Crystals of **1** diffracted poorly and the data set for **1** was 87.5% complete at $\theta = 25.267°$, limiting the accuracy of the metrical parameters. Toluene molecules in **1** and $Li_2[AIm_2]_2$ were disordered and modeled accordingly (see CIF for details). One benzene molecule in **2** was positionally disordered over two overlapping positions with 59 : 41 occupancy and refined anisotropically. Another benzene molecule in **2** exhibited partial occupancy and the occupancy of this molecule was refined freely (see CIF for details). All crystal structure diagrams were generated by ORTEP-3 for Windows (v. 2.02)[53]

Table 1 Crystallographic data for H[AIm$_2$], **1**, **2**, and Li$_2$[AIm$_2$]$_2$

Compound Lattice Solvent	H[AIm$_2$] —	**1** (Pentane)$_{0.5}$ (toluene)$_2$	**2** (Benzene)$_{3.35}$	Li$_2$[AIm$_2$]$_2$ Toluene
Empirical formula	$C_{43}H_{37}N_3$	$C_{95.50}H_{85}N_6Y$	$C_{106.09}H_{91.09}N_6Y$	$C_{46.50}H_{40}LiN_3$
Formula weight	595.76	1405.67	1538.91	647.79
Crystal system	Triclinic	Triclinic	Triclinic	Triclinic
Space group	$P\bar{1}$	$P\bar{1}$	$P\bar{1}$	$P\bar{1}$
Crystal habit	Block	Plate	Block	Block
a (Å)	7.9754(3)	13.744(2)	13.055(3)	11.8264(6)
b (Å)	12.3322(5)	14.389(2)	14.122(3)	12.7464(6)
c (Å)	17.8966(8)	20.904(3)	24.089(5)	12.7973(7)
α (°)	104.062(3)	82.938(4)	106.793(3)	101.517(3)
β (°)	101.490(2)	71.274(4)	94.276(3)	108.568(3)
γ (°)	95.503(2)	74.886(4)	98.405(3)	94.633(3)
V (Å^3)	1653.85(12)	3776.3(9)	4174.0(16)	1770.11(16)
Z	2	2	2	2
T (K)	150	100	150	100
ρ_{calcd} (g cm^{-3})	1.196	1.236	1.224	1.215
μ (mm^{-1})	0.070	0.825	0.752	0.070
R [$I_0 \geq 2\sigma(I_0)$]	0.0387	0.0697	0.0447	0.0640
R_w [$I_0 \geq 2\sigma(I_0)$]	0.0841	0.1614	0.1104	0.1479
Goodness of fit	1.0015	0.9210	0.9701	0.9830

and rendered using POV-Ray (v. 3.6.1).[54] The crystallographic data are summarized in Table 1.

Methyl 2-(*N*-(4-methylphenyl)amino)-5-methylbenzoate. This procedure was adapted from a previous report of a Buchwald–Hartwig coupling using similar substrates.[55] A solution of 4-bromotoluene (3.452 g, 20.18 mmol) and methyl-2-amino-5-methylbenzoate (3.280 g, 19.86 mmol) in toluene (20 mL) was added to a mixture of palladium(II) acetate (0.244 g, 1.09 mmol), tri-*tert*-butylphosphine (0.658 g, 3.25 mmol), and caesium carbonate (8.840 g, 27.13 mmol) in toluene (4 mL) and refluxed for 18.5 hours. The reaction mixture was allowed to cool to room temperature and then gravity filtered. The orange filtrate was concentrated under reduced pressure and the crude product was purified by silica gel column chromatography (hexanes followed by 50 : 1 hexanes : ethyl acetate) to obtain a yellow oil. Yield: 3.682 g (72.6%). Analytical and spectroscopic data for this compound have been published previously.[16]

3,6,9,9-Tetramethyl-9,10-dihydroacridine (HAH$_2$). The synthesis of HAH$_2$ has been reported,[16] however, minor modifications to the procedure are detailed here. MeMgBr (3.18 M in Et$_2$O, 12.6 mL, 40.0 mmol) was added dropwise to a solution of methyl 2-(*N*-(4-methylphenyl)amino)-5-methylbenzoate (2.554 g, 10.00 mmol) in THF (60 mL) at 0 °C, warmed to room temperature, and stirred for 15 hours. The reaction solution was added to H$_2$O (150 mL) dropwise and the product was extracted with Et$_2$O. The organic layer was collected, dried over anhydrous Na$_2$SO$_4$, and gravity filtered. The filtrate was concentrated under reduced pressure to give a yellow oil, which was used in the next step without further purification. 85% H$_3$PO$_4$ (10 mL) was added to the yellow oil and heated to 120 °C for 2.25 hours. The green reaction mixture was diluted with H$_2$O, (80 mL) extracted with Et$_2$O, and the organic phase was collected. The aqueous phase was neutralized using a 1 M NaOH solution and extracted with Et$_2$O (2 × 50 mL). All of the organic phases were combined, dried with anhydrous Na$_2$SO$_4$, and gravity filtered. Volatiles were removed from the filtrate under reduced pressure to yield a brown solid suitably pure for further reactions. Yield: 1.946 g (82.1%). Analytical and spectroscopic data for this compound have been published previously.[16]

H[AIm$_2$]. The catalyst mixture of Pd$_2$dba$_3$ (0.0927 g, 0.101 mmol), *rac*-BINAP (0.1261 g, 0.2025 mmol), and sodium *tert*-butoxide (0.6324 g, 6.580 mmol)[18a] in toluene (5 mL) was heated to 110 °C. A solution of HABr$_2$ (1.000 g, 2.531 mmol) and benzophenone imine (1.10 mL, 6.58 mmol) in toluene (20 mL) was then added to the catalyst mixture and refluxed for 16 hours. The reaction mixture was allowed to cool to room temperature, extracted with Et$_2$O (100 mL), washed with H$_2$O (150 mL), and the organic layer was collected. The aqueous layer was extracted with Et$_2$O (100 mL) twice more. The organic layers were combined and dried with MgSO$_4$, gravity filtered, and the filtrate was concentrated under reduced pressure to obtain a dark orange oil. The crude product was purified by silica gel column chromatography (CH$_2$Cl$_2$) to obtain an orange oil. A crystalline orange solid was obtained by adding a small amount of EtOH to a concentrated Et$_2$O solution of the product. The solid was washed with hexanes, collected by gravity filtration, and air dried. Yield: 1.130 g (74.8%). Crystals suitable for X-ray analysis were obtained by slow evaporation of 1 : 2 Et$_2$O/EtOH solution of the product. ^{1}H NMR (600 MHz, CD$_2$Cl$_2$, 298 K): δ 7.66 (m, 4H, Ph*H*), 7.41 (br s, 1H, N*H*), 7.30–7.35 (m, 8H, Ph*H*), 7.18 (m, 4H, Ph*H*), 7.11 (m, 4H, Ph*H*), 6.84 (br s, 2H, C*H*^{1,8}), 6.00 (m, 2H, C*H*^{3,6}), 2.02 (s, 6H, Ar*Me*), 1.50 (s, 6H, C*Me*$_2$). ^{13}C{^{1}H} NMR (151 MHz, CD$_2$Cl$_2$, 298 K): δ 169.0 (N=*C*), 139.7 (N=C–*C*), 137.2 (N=C–*C*), 135.8 (*C*^{12,13}), 130.82 (Ph*C*), 130.78 (*C*^{4,5}), 129.5 (*C*^{11,14}), 129.3 (Ph*C*), 129.2 (Ph*C*), 129.0 (Ph*C*), 128.5 (Ph*C*), 128.3 (C^{2,7}), 121.7 (C*H*^{1,8}),

118.4 (C$H^{3,6}$), 36.8 (*C*Me$_2$), 30.0 (C*Me*$_2$), 21.1 (Ar*Me*). UV-vis (benzene): λ_{max} (ε) = 438 nm (4640). Anal. Calcd for $C_{43}H_{37}N_3$: C, 86.69; H, 6.26; N, 7.05. Found: C, 86.45; H, 6.38; N, 6.97.

Compound 1. Y(CH$_2$SiMe$_3$)$_3$(THF)$_2$ (0.050 g, 0.101 mmol) and H[AIm$_2$] (0.120 g, 0.202 mmol) were stirred in benzene (6 mL) at room temperature to give a dark blue solution. Volatiles were removed *in vacuo* after 30 minutes and a dark blue solid was collected. A saturated solution of the crude product was prepared in toluene and filtered through Celite to remove any undissolved solids. The crude product was recrystallized by layering pentane onto the saturated toluene solution in several sealed culture tubes and cooling to −30 °C. Yield: 0.110 g (84.9%). ^{1}H NMR (500 MHz, d$_8$-toluene, 238 K): δ 8.83 (d, $^3J_{H,H}$ 7 Hz, 1H, C$_6H_4$ *ortho* to metalated carbon atom), 7.56 (d, $^3J_{H,H}$ 7 Hz, 4H, *o*-Ph*H* intact AIm$_2$), 7.28 (t, $^3J_{H,H}$ 7 Hz, 1H, C$_6H_4$ *meta* to metalated carbon atom), 7.25 (d, $^3J_{H,H}$ 7 Hz, 2H, *o*-Ph*H* metalated AIm$_2$), 7.2–6.7 (m, 29H, PhH), 6.91 (2H, C$H^{1,8}$ intact AIm$_2$), 6.81, 6.72 (2 × 1H, CH^1 and CH^8 on metalated AIm$_2$), 6.60 (d, $^3J_{H,H}$ 7 Hz, 2H, *o*-Ph*H* metalated AIm$_2$), 5.94 (s, 2H, C$H^{3,6}$ intact AIm$_2$), 5.92, 5.42 (s, 2 × 1H, CH^3 and CH^6 on metalated AIm$_2$), 2.04, 1.84 (s, 2 × 3H, C*Me*$_2$ intact AIm$_2$), 1.99 {s, 9H, Ar*Me* intact AIm$_2$ (6H) + Ar*Me* metalated AIm$_2$ (3H)}, 1.80 {s, 9H, C*Me*$_2$ metalated AIm$_2$ (6H) + Ar*Me* metalated AIm$_2$ (3H)}. ^{13}C{^{1}H} NMR (125 MHz, d$_8$-toluene, 238 K): δ 194.20 (d, $^1J_{13C,89Y}$ 42.7 Hz, *ipso* Y–*C*$_6$H$_4$), 178.47, 174.21, 169.51 (3 × N═*C*), 139.89 (Ar–*C*H *ortho* to metalated carbon), 140.81, 131.15, 130.87, 130.60, 130.42, 129.86, 129.52, 128.68, 128.44, 127.56, 127.23, 126.69, 125.77, 124.58, 124.48, 124.07, 123.16, 122.79 {18 × Ar–*C*H (expected 24)}, 151.39, 145.81, 144.55, 142.84, 142.50, 141.71, 140.71, 139.82, 139.41, 137.70, 134.06, 130.59, 130.01, 126.92, 123.81, 122.82, 120.60 {17 × quaternary Ar (expected 18)}, 40.59, 28.43 (2 × C*Me*$_2$ intact AIm$_2$), 36.57 (*C*Me$_2$ intact AIm$_2$), 36.02 (*C*Me$_2$ metalated AIm$_2$), 35.88 (C*Me*$_2$ metalated AIm$_2$), 21.60, 20.50 (Ar*Me* metalated AIm$_2$), 21.22 (Ar*Me* intact AIm$_2$). UV-vis (benzene): λ_{max} (ε) = 637 nm (7911). Anal. Calcd for $C_{91}H_{83}N_6Y$ (**1**·pentane): C, 80.99; H, 6.20; N, 6.23. Found: C, 80.91; H, 6.24; N, 6.19.

Compound 2. Y(CH$_2$SiMe$_3$)$_3$(THF)$_2$ (0.050 g, 0.101 mmol) and H[AIm$_2$] (0.120 g, 0.202 mmol) were stirred in benzene (5 mL) at room temperature to give a dark blue solution that slowly changed to dark green-brown over the course of three days. Volatiles were removed *in vacuo* and a dark green-brown crystalline solid was collected. A saturated solution of the crude product was prepared in benzene and filtered through Celite to remove any undissolved solids. The crude product was recrystallized by layering pentane onto the saturated benzene solution in several sealed culture tubes. Yield: 117.5 mg (91.3%). ^{1}H NMR (600 MHz, C$_6$D$_6$, 298 K): δ 8.79 (broad d, $^3J_{H,H}$ 7 Hz, 1H, *o*-C$_6H_5$ A), 8.21 (broad d, $^3J_{H,H}$ 6 Hz, 1H, *o*-Ar*H* B), 8.13 (d, $^3J_{H,H}$ 7.5 Hz, 1H, *o*-Ar*H* C), 7.79 (broad t, $^3J_{H,H}$ 7 Hz, 1H, *m*-C$_6H_5$ A), 7.51 (broad s, 2H, Ar*H*), 7.45 (broad d, $^3J_{H,H}$ 7 Hz, 1H, *o*-C$_6H_5$ A), 7.2 (very broad s, 2H, Ar*H*), 7.20 (broad d, $^3J_{H,H}$ 7.5 Hz, 1H, *o*-Ar*H* B), 7.1–6.8 (m, 21H, Ar*H*), 6.99 (s, 1H, C$H^{1/8}$ α), 6.92 (broad t, $^3J_{H,H}$ 7 Hz, 1H, *m*-C$_6H_5$ A), 6.86 (broad t, $^3J_{H,H}$ 8 Hz, 1H, *p*-C$_6H_5$ A), 6.77 (very broad s, 4H, Ar*H*), 6.58 (s, 1H, C$H^{1/8}$ β), 6.55 (d, $^3J_{H,H}$ 7.5 Hz, 2H, *o*-Ar–*H*), 6.46 (s, 1H, C$H^{1/8}$ γ), 6.33 (s, 1H, C$H^{1/8}$ δ), 6.22 (s, 1H, C$H^{3/6}$ α), 5.84 (s, 1H, C$H^{3/6}$ β), 5.82 (s, 1H, C$H^{3/6}$ δ), 5.15 (s, 1H, C$H^{3/6}$ γ), 2.26 (s, 3H, ArMe δ), 2.01 (s, 3H, ArMe α), 1.73 (s, 3H, ArMe β), 1.66 (s, 3H, ArMe γ), 1.87, 1.34 (s, 2 × 3H, one C*Me*$_2$), 1.57, 1.33 (s, 2 × 3H, one C*Me*$_2$). ^{13}C{^{1}H} NMR (151 MHz, C$_6$D$_6$, 298 K): δ 180.63, 164.91 (2 × N═*C*), 149.34, 148.64, 147.76, 147.47, 143.82, 143.39, 142.74, 142.56, 140.73, 140.27, 140.17, 140.07, 137.85, 135.63, 135.35, 132.91, 130.08, 126.31, 126.13, 124.91, 124.54, 121.56, 121.47 {23 × quaternary Ar (expected 25)}, 134.71 (*m*-C$_6H_5$ A), 133.99 (*C*H$^{3/6}$ γ), 131.21, 131.10, 130.50, 130.26, 130.17, 130.03, 129.87, 129.52, 129.46, 128.73, 128.70, 128.34, 128.11, 127.82, 127.72, 127.38, 127.19, 126.95, 126.90, 126.59, 126.55, 126.02 {22 × Ar–*C*H (expected 31)}, 124.26 (*C*H$^{1/8}$ β), 122.01 (*C*H$^{3/6}$ α), 121.73 (*C*H$^{1/8}$ γ), 121.05 (*C*H$^{3/6}$ β), 113.89 (*C*H$^{3/6}$ δ), 113.86 (*C*H$^{1/8}$ δ), 100.38, 84.45 (isoindoline *C*Ph$_2$ and *C*PhNAr), 39.97, 27.56 (2 × one C*Me*$_2$), 36.38, 36.32 (2 × *C*Me$_2$), 36.25, 31.01 (2 × one C*Me*$_2$), 22.31 (Ar*Me* δ), 21.42 (Ar*Me* α), 20.61 (Ar*Me* β), 20.40 (Ar*Me* γ). UV-vis (benzene): λ_{max} (ε) = 898 nm (3299). Anal. Calcd for $C_{104}H_{89}N_6Y$ (**2**·3benzene): C, 82.63; H, 5.93; N, 5.56. Found: C, 82.51; H, 6.03; N, 5.58.

Li$_x$[AIm$_2$]$_x$ (*x* = 2 in the solid state). LiCH$_2$SiMe$_3$ (0.0158 g, 0.168 mmol) and H[AIm$_2$] (0.1000 g, 0.1679 mmol) were stirred in toluene (10 mL) at room temperature to give a dark blue solution. Volatiles were removed *in vacuo* after 1.5 hours and a dark blue solid was collected. A concentrated solution of the crude product was prepared in toluene and filtered through Celite to remove any undissolved solids. The crude product was recrystallized by layering pentane onto the toluene solution and cooling to −30 °C. Yield: 73.3 mg (72.6%). ^{1}H NMR (600 MHz, C$_6$D$_6$, 298 K): δ 7.17 (d, $^3J_{H,H}$ 7 Hz, 4H, *o*-Ph*H* B), 7.15 (s, 2H, C$H^{1,8}$), 7.06 (d, $^3J_{H,H}$ 7 Hz, 4H, *o*-Ph*H* A), 6.98 (t, $^3J_{H,H}$ 7 Hz, 2H, *p*-Ph*H* A), 6.95 (t, $^3J_{H,H}$ 7 Hz, 2H, *p*-Ph*H* B), 6.91 (t, $^3J_{H,H}$ 7 Hz, 4H, *m*-Ph*H* B), 6.82 (t, $^3J_{H,H}$ 7 Hz, 4H, *m*-Ph*H* A), 6.27 (s, 2H, C$H^{3,6}$), 2.14 (s, 6H, Ar*Me*), 1.88 (s, 6H, C*Me*$_2$). ^{13}C{^{1}H} NMR (151 MHz, C$_6$D$_6$, 298 K): δ 164.01 (N═*C*), 146.96 (*C*^{12,13}), 142.85 (*ipso*-Ph*C* A), 137.88 (*ipso*-Ph*C* B), 137.18 (*C*^{4,5}), 132.15 (C^{11,14}), 130.16 (*o*-Ph*C* B), 129.44 (*p*-Ph*C* A), 128.98 (*m*-Ph*C* A), 128.95 (*p*-Ph*C* B), 128.35 (down *m*-Ph*C*), 128.02 (up *o*-Ph*C*), 125.07 (*C*H^{1,8}), 121.43 (*C*^{2,7}), 120.23 (*C*H^{3,6}), 37.60 (*C*(CH$_3$)$_2$), 31.85 (C*Me*$_2$), 21.64 (Ar*Me*). UV-vis (benzene): λ_{max} (ε) = 654 nm (7889). Anal. Calcd for $C_{50}H_{44}LiN_3$ (Li[AIm$_2$]·toluene): C, 86.55; H, 6.39; N, 6.06. Found: C, 86.35; H, 6.46; N, 6.14.

Acknowledgements

D. J. H. E. thanks NSERC of Canada for a Strategic Project Grant.

References

1 K. R. D. Johnson and P. G. Hayes, *Chem. Soc. Rev.*, 2013, **42**, 1947.

2 (*a*) D. J. H. Emslie, W. E. Piers and M. Parvez, *Dalton Trans.*, 2003, 2615; (*b*) M. Zimmermann, K. W. Tornroos and

R. Anwander, *Angew. Chem., Int. Ed.*, 2007, **46**, 3126; (*c*) G. Zhang, Y. Wei, L. Guo, X. Zhu, S. Wang, S. Zhou and X. Mu, *Chem. – Eur. J.*, 2015, **21**, 2519; (*d*) K. L. Miller, B. N. Williams, D. Benitez, C. T. Carver, K. R. Ogilby, E. Tkatchouk, W. A. Goddard III and P. L. Diaconescu, *J. Am. Chem. Soc.*, 2010, **132**, 342.

3 (*a*) C. A. Cruz, D. J. H. Emslie, L. E. Harrington, J. F. Britten and C. M. Robertson, *Organometallics*, 2007, **26**, 692; (*b*) C. A. Cruz, D. J. H. Emslie, L. E. Harrington and J. F. Britten, *Organometallics*, 2008, **27**, 15; (*c*) C. A. Cruz, D. J. H. Emslie, H. A. Jenkins and J. F. Britten, *Dalton Trans.*, 2010, **39**, 6626; (*d*) N. R. Andreychuk, S. Ilango, B. Vidjayacoumar, D. J. H. Emslie and H. A. Jenkins, *Organometallics*, 2013, **32**, 1466.

4 C. A. Cruz, D. J. H. Emslie, C. M. Robertson, L. E. Harrington, H. A. Jenkins and J. F. Britten, *Organometallics*, 2009, **28**, 1891.

5 (*a*) W. E. Piers and D. J. H. Emslie, *Coord. Chem. Rev.*, 2002, **233**, 131; (*b*) J. Gromada, J. F. Carpentier and A. Mortreux, *Coord. Chem. Rev.*, 2004, **248**, 397; (*c*) P. M. Zeimentz, S. Arndt, B. R. Elvidge and J. Okuda, *Chem. Rev.*, 2006, **106**, 2404; (*d*) Z. Hou, Y. Luo and X. Li, *J. Organomet. Chem.*, 2006, **691**, 3114; (*e*) T. Li, J. Jenter and P. W. Roesky, in *Rare-Earth Metal Postmetallocene Catalysts with Chelating Amido Ligands - Molecular Catalysis of Rare-Earth Elements*, ed. P. W. Roesky, 2010, vol. 137, p. 165; (*f*) A. A. Trifonov, *Coord. Chem. Rev.*, 2010, **254**, 1327; (*g*) M. Nishiura and Z. Hou, *Nat. Chem.*, 2010, **2**, 257; (*h*) F. T. Edelmann, *Chem. Soc. Rev.*, 2012, **41**, 7657.

6 (*a*) G. A. Molander and J. A. C. Romero, *Chem. Rev.*, 2002, **102**, 2161; (*b*) S. Hong and T. J. Marks, *Acc. Chem. Res.*, 2004, **37**, 673; (*c*) T. E. Mueller, K. C. Hultzsch, M. Yus, F. Foubelo and M. Tada, *Chem. Rev.*, 2008, **108**, 3795; (*d*) Ref. 7.

7 A. L. Reznichenko and K. C. Hultzsch, in *Catalytic sigma-Bond Metathesis - Molecular Catalysis of Rare-Earth Elements*, ed. P. W. Roesky, 2010, vol. 137, p. 1.

8 C. A. Cruz, T. Chu, D. J. H. Emslie, H. A. Jenkins, L. E. Harrington and J. F. Britten, *J. Organomet. Chem.*, 2010, **695**, 2798.

9 (*a*) A. M. Neculai, H. W. Roesky, D. Neculai and J. Magull, *Organometallics*, 2001, **20**, 5501; (*b*) T. M. Cameron, J. C. Gordon, R. Michalczyk and B. L. Scott, *Chem. Commun.*, 2003, 2282; (*c*) N. Meyer and P. W. Roesky, *Z. Anorg. Allg. Chem.*, 2008, **634**, 2171; (*d*) E. Lu, Y. Chen and X. Leng, *Organometallics*, 2011, **30**, 5433; (*e*) E. Lu, Y. Chen, J. Zhou and X. Leng, *Organometallics*, 2012, **31**, 4574; (*f*) Z. Feng, X. Zhu, S. Wang, S. Wang, S. Zhou, Y. Wei, G. Zhang, B. Deng and X. Mu, *Inorg. Chem.*, 2013, **52**, 9549. For related ligands (not included in Fig. 2) in which the "imine" donor is part of a pyrazole or thiazole ring, see: (*g*) K. R. D. Johnson, B. L. Kamenz and P. G. Hayes, *Organometallics*, 2014, **33**, 3005; (*h*) D. M. Lyubov, L. Luconi, A. Rossin, G. Tuci, A. V. Cherkasov, G. K. Fukin, G. Giambastiani and A. A. Trifonov, *Chem. – Eur. J.*, 2014, **20**, 3487; (*i*) L. Luconi, D. M. Lyubov, A. Rossin, T. A. Glukhova, A. V. Cherkasov, G. Tuci, G. K. Fukin, A. A. Trifonov and G. Giambastiani, *Organometallics*, 2014, **33**, 7125.

10 (*a*) F. Lauterwasser, P. G. Hayes, S. Brase, W. E. Piers and L. L. Schafer, *Organometallics*, 2004, **23**, 2234; (*b*) L. Xiang, Q. Wang, H. Song and G. Zi, *Organometallics*, 2007, **26**, 5323; (*c*) H. Kaneko, H. Tsurugi, T. K. Panda and K. Mashima, *Organometallics*, 2010, **29**, 3463; (*d*) F. Lauterwasser, P. G. Hayes, W. E. Piers, L. L. Schafer and S. Bräse, *Adv. Synth. Catal.*, 2011, **353**, 1384.

11 (*a*) Y. Matsuo, K. Mashima and K. Tani, *Organometallics*, 2001, **20**, 3510; (*b*) W. Gao, D. Cui, X. Liu, Y. Zhang and Y. Mu, *Organometallics*, 2008, **27**, 5889; (*c*) L. F. Sánchez-Barba, D. L. Hughes, S. M. Humphrey and M. Bochmann, *Organometallics*, 2005, **24**, 3792; (*d*) X. Liu, X. Shang, T. Tang, N. Hu, F. Pei, D. Cui, X. Chen and X. Jing, *Organometallics*, 2007, **26**, 2747; (*e*) X. Shang, X. Liu and D. Cui, *J. Polym. Sci., Part A: Polym. Chem.*, 2007, **45**, 5662; (*f*) G. Du, Y. Wei, W. Zhang, Y. Dong, Z. Lin, H. He, S. Zhang and X. Li, *Dalton Trans.*, 2013, **42**, 1278.

12 M. Cui, A. Shafir, C. L. Reeder and J. Arnold, *Organometallics*, 2003, **22**, 3357.

13 (*a*) Y. Yang, B. Liu, K. Lv, W. Gao, D. Cui, X. Chen and X. Jing, *Organometallics*, 2007, **26**, 4575; (*b*) Y. Yang, Q. Wang and D. Cui, *J. Polym. Sci., Part A: Polym. Chem.*, 2008, **46**, 5251; (*c*) G. Du, Y. Wei, L. Ai, Y. Chen, Q. Xu, X. Liu, S. Zhang, Z. Hou and X. Li, *Organometallics*, 2010, **30**, 160; (*d*) D. Li, S. Li, D. Cui and Z. Zhang, *Organometallics*, 2010, **29**, 2186; (*e*) H. Liu, J. He, Z. Liu, Z. Lin, G. Du, S. Zhang and X. Li, *Macromolecules*, 2013, **46**, 3257.

14 (*a*) P. G. Hayes, W. E. Piers and R. McDonald, *J. Am. Chem. Soc.*, 2002, **124**, 2132; (*b*) M. Zimmermann, K. W. Törnroos, R. M. Waymouth and R. Anwander, *Organometallics*, 2008, **27**, 4310.

15 (*a*) L. W. M. Lee, W. E. Piers, M. R. J. Elsegood, W. Clegg and M. Parvez, *Organometallics*, 1999, **18**, 2947; (*b*) P. G. Hayes, W. E. Piers and M. Parvez, *J. Am. Chem. Soc.*, 2003, **125**, 5622; (*c*) P. G. Hayes, G. C. Welch, D. J. H. Emslie, C. L. Noack, W. E. Piers and M. Parvez, *Organometallics*, 2003, **22**, 1577; (*d*) P. G. Hayes, W. E. Piers and M. Parvez, *Organometallics*, 2005, **24**, 1173; (*e*) A. L. Kenward, W. E. Piers and M. Parvez, *Organometallics*, 2009, **28**, 3012; (*f*) A. L. Kenward, J. A. Ross, W. E. Piers and M. Parvez, *Organometallics*, 2009, **28**, 3625.

16 H. Liu, N.-D. Wang and D.-M. Du, *Lett. Org. Chem.*, 2010, **7**, 114.

17 C. P. A. T. Lawson, A. M. Z. Slawin and N. J. Westwood, *Chem. Commun.*, 2011, **47**, 1057.

18 (*a*) F. M. Rivas, A. J. Giessert and S. T. Diver, *J. Org. Chem.*, 2002, **67**, 1708; (*b*) J. P. Wolfe, J. Åhman, J. P. Sadighi, R. A. Singer and S. L. Buchwald, *Tetrahedron Lett.*, 1997, **38**, 6367.

19 F. H. Allen, O. Kennard, D. G. Watson, L. Brammer, A. G. Orpen and R. Taylor, *J. Chem. Soc., Perkin Trans. 2*, 1987, S1.

20 F. Estler, G. Eickerling, E. Herdtweck and R. Anwander, *Organometallics*, 2003, **22**, 1212.
21 M. D. Rausch, D. F. Foust, R. D. Rogers and J. L. Atwood, *J. Organomet. Chem.*, 1984, **265**, 241.
22 E. Lu, W. Gan and Y. Chen, *Dalton Trans.*, 2011, **40**, 2366.
23 B. Liu, X. Liu, D. Cui and L. Liu, *Organometallics*, 2009, **28**, 1453.
24 D. M. Lyubov, G. K. Fukin, A. V. Cherkasov, A. S. Shavyrin, A. A. Trifonov, L. Luconi, C. Bianchini, A. Meli and G. Giambastiani, *Organometallics*, 2009, **28**, 1227.
25 A. R. Petrov, K. A. Rufanov, K. Harms and J. Sundermeyer, *J. Organomet. Chem.*, 2009, **694**, 1212.
26 X. Gu, X. Zhu, Y. Wei, S. Wang, S. Zhou, G. Zhang and X. Mu, *Organometallics*, 2014, **33**, 2372.
27 D. Cui, M. Nishiura and Z. Hou, *Angew. Chem., Int. Ed.*, 2005, **44**, 959.
28 Y. Obora, T. Ohta, C. L. Stern and T. J. Marks, *J. Am. Chem. Soc.*, 1997, **119**, 3745.
29 F. Zhou, M. Lin, L. Li, X. Zhang, Z. Chen, Y. Li, Y. Zhao, J. Wu, G. Qian, B. Hu and W. Li, *Organometallics*, 2011, **30**, 1283.
30 R. Shannon, *Acta Crystallogr., Sect. A: Cryst. Phys., Diffr., Theor. Gen. Cryst.*, 1976, **32**, 751.
31 W. Zhang, S. Liu, W. Yang, X. Hao, R. Glaser and W.-H. Sun, *Organometallics*, 2012, **31**, 8178.
32 (*a*) L. Wan, D. Zhang, Q. Wang, Z. Chen and L. Weng, *J. Organomet. Chem.*, 2013, **724**, 155; (*b*) J. Wang, L. Wan, D. Zhang, Q. Wang and Z. Chen, *Eur. J. Inorg. Chem.*, 2013, 2093.
33 E. Lu, Y. Chen and X. Leng, *Organometallics*, 2011, **30**, 5433.
34 M. E. G. Skinner and P. Mountford, *J. Chem. Soc., Dalton Trans.*, 2002, 1694.
35 (*a*) G. A. Grasa, M. S. Viciu, J. Huang and S. P. Nolan, *J. Org. Chem.*, 2001, **66**, 7729; (*b*) G. Mann, J. F. Hartwig, M. S. Driver and C. Fernández-Rivas, *J. Am. Chem. Soc.*, 1998, **120**, 827.
36 S. Fergus, S. J. Eustace and A. F. Hegarty, *J. Org. Chem.*, 2004, **69**, 4663.
37 D. J. H. Emslie, W. E. Piers, M. Parvez and R. McDonald, *Organometallics*, 2002, **21**, 4226.
38 K. Okuno, Y. Shigeta, R. Kishi, H. Miyasaka and M. Nakano, *J. Photochem. Photobiol., A*, 2012, **235**, 29.
39 A. Hagfeldt, G. Boschloo, L. Sun, L. Kloo and H. Pettersson, *Chem. Rev.*, 2010, **110**, 6595.
40 J. F. Van der Maelen Uria, S. K. Pandey, H. W. Roesky and G. M. Sheldrick, *Acta Crystallogr., Sect. C: Cryst. Struct. Commun.*, 1994, **50**, 671.
41 M. Veith, A. Koban, K. Fries, P. Spaniol, R. Elsässer, A. Rammo, V. Huch and U. Kleinsteuber, *Organometallics*, 1998, **17**, 2612.
42 G. R. Fulmer, A. J. M. Miller, N. H. Sherden, H. E. Gottlieb, A. Nudelman, B. M. Stoltz, J. E. Bercaw and K. I. Goldberg, *Organometallics*, 2010, **29**, 2176.
43 R. M. Acheson, *The Chemistry of Heterocyclic Compounds: Acridines*, John Wiley & Sons, Toronto, 2nd edn, 1973.
44 M. J. Frisch, G. W. Trucks, H. B. Schlegel, G. E. Scuseria, M. A. Robb, J. R. Cheeseman, G. Scalmani, V. Barone, B. Mennucci, G. A. Petersson, H. Nakatsuji, M. Caricato, X. Li, H. P. Hratchian, A. F. Izmaylov, J. Bloino, G. Zheng, J. L. Sonnenberg, M. Hada, M. Ehara, K. Toyota, R. Fukuda, J. Hasegawa, M. Ishida, T. Nakajima, Y. Honda, O. Kitao, H. Nakai, T. Vreven, J. A. Montgomery Jr., J. E. Peralta, F. Ogliaro, M. Bearpark, J. J. Heyd, E. Brothers, K. N. Kudin, V. N. Staroverov, R. Kobayashi, J. Normand, K. Raghavachari, A. Rendell, J. C. Burant, S. S. Iyengar, J. Tomasi, M. Cossi, N. Rega, N. J. Millam, M. Klene, J. E. Knox, J. B. Cross, V. Bakken, C. Adamo, J. Jaramillo, R. Gomperts, R. E. Stratmann, O. Yazyev, A. J. Austin, R. Cammi, C. Pomelli, J. W. Ochterski, R. L. Martin, K. Morokuma, V. G. Zakrzewski, G. A. Voth, P. Salvador, J. J. Dannenberg, S. Dapprich, A. D. Daniels, Ö. Farkas, J. B. Foresman, J. V. Ortiz, J. Cioslowski and D. J. Fox, *Gaussian 09, Revision D.01*, Gaussian, Inc., Wallingford, CT, 2009.
45 T. Yanai, D. Tew and N. Handy, *Chem. Phys. Lett.*, 2004, **393**, 51.
46 (*a*) G. A. Petersson, A. Bennett, T. G. Tensfeldt, M. A. Al-Laham, W. A. Shirley and J. Mantzaris, *J. Chem. Phys.*, 1988, **89**, 2193; (*b*) G. A. Petersson and M. A. J. Al-Laham, *Chem. Phys.*, 1991, **94**, 6081.
47 (*a*) P. J. Hay and W. R. Wadt, *J. Chem. Phys.*, 1985, **82**, 270; (*b*) P. J. Hay and W. R. Wadt, *J. Chem. Phys.*, 1985, **82**, 299; (*c*) W. R. Wadt and P. J. Hay, *J. Chem. Phys.*, 1985, **82**, 284.
48 (*a*) R. E. Stratmann, G. E. Scuseria and M. J. Frisch, *J. Chem. Phys.*, 1998, **109**, 8218; (*b*) G. Scalmani, M. J. Frisch, B. Mennucci, J. Tomasi, R. Cammi and V. Barone, *J. Chem. Phys.*, 2006, **124**, 1.
49 (*a*) S. Miertuš, E. Scrocco and J. Tomasi, *Chem. Phys.*, 1981, **55**, 117; (*b*) S. Miertuš and J. Tomasi, *Chem. Phys.*, 1982, **65**, 239; (*c*) J. L. Pascual-Ahuir, E. Silla and I. Tuñón, *J. Comput. Chem.*, 1994, **15**, 1127; (*d*) J. Tomasi, B. Mennucci and R. Cammi, *Chem. Rev.*, 2005, **105**, 2999.
50 S. I. Gorelsky, *AOMix-Software Package for Electronic Structure Analysis, Revision 6.87d*, Ottawa, ON, 2013.
51 A. Altomare, G. Cascarano, C. Giacovazzo, A. Guagliardi, M. C. Burla, G. Polidori and M. Camalli, *J. Appl. Crystallogr.*, 1994, **27**, 435.
52 P. W. Betteridge, J. R. Carruthers, R. I. Cooper, K. Prout and D. J. Watkin, *J. Appl. Crystallogr.*, 2003, **36**, 1487.
53 L. J. Farrugia, *J. Appl. Crystallogr.*, 1997, **30**, 565.
54 *Persistence of Vision Raytracer, Version 3.6.1*, Persistence of Vision Pty. Ltd, Williamstown, VIC, Australia, 2004.
55 H. Bertrand, A. Granzhan, D. Monchaud, N. Saettel, R. Guillot, S. Clifford, A. Guédin, J.-T. Mergny and M.-P. Teulade-Fichou, *Chem. – Eur. J.*, 2011, **17**, 4529.

